A Regime Perspective on the North Atlantic Eddy-Driven Jet Response to Sudden Stratospheric Warmings

AMANDA C. MAYCOCK

School of Earth and Environment, University of Leeds, Leeds, United Kingdom

GIBBON I. T. MASUKWEDZA[a]

School of Earth and Environment, University of Leeds, Leeds, United Kingdom, and Zimbabwe Meteorological Services Department, Harare, Zimbabwe

PETER HITCHCOCK

Department of Earth and Atmospheric Sciences, Cornell University, Ithaca, New York

ISLA R. SIMPSON

Climate and Global Dynamics Laboratory, National Center for Atmospheric Research, Boulder, Colorado

(Manuscript received 24 September 2019, in final form 11 February 2020)

ABSTRACT

Changes to the preferred states, or regime behavior, of the North Atlantic eddy-driven jet (EDJ) following a major sudden stratospheric warming (SSW) is examined using a large ensemble experiment from the Canadian Middle Atmosphere Model in which the stratosphere is nudged toward an SSW. In the 3 months following the SSW (January–March), the North Atlantic EDJ shifts equatorward by ~3°, on average; this arises from an increased occurrence of the EDJ's south regime and reductions in its north and central regimes. Qualitatively similar behavior is shown in a reanalysis dataset. We show that under SSW conditions the south regime becomes more persistent and that this can explain the overall increase in the EDJ latitude decorrelation time scale. A cluster analysis reveals that, following the SSW, the south EDJ regime is characterized by weaker low-level baroclinicity and eddy heat fluxes in the North Atlantic Ocean. We hypothesize, therefore, that the increased persistence of the south regime is related to the weaker baroclinicity leading to slower growth rates of the unstable modes and hence a slower buildup of eddy heat flux, which has been shown to precede EDJ transitions. In the North Atlantic sector, the surface response to the SSW projects onto a negative North Atlantic Oscillation (NAO) pattern, with almost no change in the east Atlantic (EA) pattern. This behavior appears to be distinct from the modeled intrinsic variability in the EDJ, where the jet latitude index captures variations in both the NAO and EA patterns. The results offer new insight into the mechanisms for stratosphere–troposphere coupling following SSWs.

1. Introduction

Observations and model studies show that, on average, the North Atlantic eddy-driven jet (EDJ) temporarily moves equatorward following major sudden stratospheric warmings (SSWs) (e.g., Baldwin and Dunkerton 2001; Charlton and Polvani 2007; Hitchcock and Simpson 2014, hereinafter HS14). The EDJ shift is associated with a more negative phase of the North Atlantic Oscillation (NAO) and contributes to enhanced predictive skill of winter climate in the Euro-Atlantic region (Scaife and Knight 2008; Sigmond et al. 2013; Fereday et al. 2012; Scaife et al. 2016; Tripathi et al. 2015). While much attention has been paid to the tropospheric response to SSWs on monthly to seasonal time scales (e.g., Charlton and Polvani 2007; Polvani

[a] Current affiliation: Department of Geography, University of Sussex, Brighton, United Kingdom.

Corresponding author: Amanda C. Maycock, a.c.maycock@leeds.ac.uk

DOI: 10.1175/JCLI-D-19-0702.1

et al. 2017), few studies have assessed whether there are accompanying changes in variability in the North Atlantic EDJ. Such changes could help to contextualize the mechanisms for the time mean circulation response and may also be important for the occurrence of extreme weather events following SSWs (Kolstad et al. 2010). Charlton-Perez et al. (2018) analyzed daily North Atlantic weather regimes and showed that when the stratospheric polar vortex is anomalously weak, the likelihood of the subsequent day being in a negative NAO state is approximately doubled relative to neutral polar vortex days. They showed that this was related to both increased persistence of the NAO negative state and an increased likelihood for transitions from other weather regimes to the NAO negative state. Here we focus on understanding the influence of SSWs on the latitude of the North Atlantic EDJ.

The winter daily EDJ latitude in the North Atlantic sector exhibits a trimodal structure corresponding to north, central, and south preferred jet locations (Woollings et al. 2010a). There has been extensive discussion in the literature about whether multimodal structures in the midlatitude circulation reflect true dynamical regimes (e.g., Charney and DeVore 1979; Silverman 1981; Corti et al. 1999; Ambaum 2008; Woollings et al. 2010b; Smyth et al. 1999; Hannachi 2007; Franzke et al. 2009). In this study, for simplicity, we refer to the peaks of the North Atlantic jet latitude distribution as regime states.

One interpretation of the trimodal distribution of the EDJ latitude is that the peaks are linked to the occurrence or absence of atmospheric blocking. The southern jet regime is associated with Greenland blocking (Woollings et al. 2008, 2010b). The central jet regime can be interpreted as an undisturbed state with separate subtropical and eddy-driven jets (Woollings et al. 2010a). The interpretation of the northern jet regime is less clear (Woollings et al. 2010a), but the presence of Greenland may be important through orographic forcing of tip jets (White et al. 2019), as is the development of a strong and persistent ridge in the subtropics through anticyclonic wave breaking near the Iberian Peninsula (Woollings et al. 2011).

It has been proposed that the transitions between the three jet regimes can be understood from a nonlinear oscillator relationship between the meridional temperature gradient (i.e., baroclinicity) and the meridional eddy heat flux, which acts to erode baroclinicity through storm-track activity (Ambaum and Novak 2014; Novak et al. 2015). In a period of low storm-track activity, baroclinicity will increase through diabatic processes. This will favor the development of coherent eddies and cyclonic wave breaking, which steers the jet south. As the eddies become more vigorous and propagate farther downstream, the enhanced eddy deformation will favor anticyclonic wave breaking, which steers the jet poleward. Continued eddy mixing reduces the baroclinicity and inhibits new storm formation, further favoring anticyclonic wave breaking and a northward deflection of the jet as the ridge in the eastern Atlantic strengthens. As the eddy activity decays in the low baroclinicity environment, the baroclinicity will start to be replenished through diabatic processes and the cycle begins again (Novak et al. 2015; Franzke et al. 2011). Shifts in EDJ latitude over this recharge–discharge cycle of baroclinicity and storm-track activity occur downstream as a result of the varying baroclinicity affecting eddy anisotropy and wave breaking characteristics (Orlanski 2003).

Cluster analysis shows that the three regimes of the North Atlantic jet latitude exhibit different persistence characteristics, with the southward regime being, on average, more persistent than the northward regime (Frame et al. 2011; Franzke et al. 2011; Barnes and Hartmann 2010a). Such variations in persistence of the EDJ regimes may also be related to eddy anisotropy, with a more poleward jet favoring wave breaking on the equatorward flank of the jet, reduced positive eddy–mean flow feedback and greater transience (Barnes et al. 2010; Barnes and Hartmann 2010b). Variations in the persistence of the EDJ regimes introduces the possibility of state-dependent predictability, which may be useful for weather and subseasonal prediction (Frame et al. 2013).

An immediate question is how does the trimodal structure of the EDJ latitude relate to the leading modes of North Atlantic circulation variability like the NAO and East Atlantic (EA) patterns? Together the NAO and EA patterns capture fluctuations in both EDJ latitude and speed (Woollings et al. 2010a), similar to the behavior seen in idealized models for the jet (Monahan and Fyfe 2006; Sparrow et al. 2009), although there is a general tendency that for negative NAO days the EDJ is anomalously south (Woollings et al. 2010a). Another feature of note is the negative skewness of the winter daily NAO distribution. Woollings et al. (2010b) explain this skewness in terms of two flow regimes representing Greenland blocking and a subpolar jet. However, the NAO alone cannot explain the full variability in EDJ latitude. Much remains to be learned about how the North Atlantic EDJ regimes relate to other common hemispheric-scale measures of the midlatitude circulation, such as the annular modes and NAO.

The growing literature on North Atlantic EDJ regimes and their relationship to jet variability and predictability is largely disconnected from the literature

on sudden stratospheric warming (SSW) impacts on surface climate. Despite the fact that the observed surface response to SSWs is largest in the North Atlantic sector (Charlton and Polvani 2007), much of the research into stratosphere–troposphere coupling has used zonally symmetric idealized models (e.g., Gerber et al. 2009; Polvani and Kushner 2002; Kushner and Polvani 2004) and hemispheric-scale quantities like the NAM (e.g., Baldwin and Dunkerton 2001), which has important distinctions from the NAO (Ambaum et al. 2001). Much less attention has been paid to understanding the connections between the zonal mean and regional North Atlantic aspects of the surface climate response following SSWs. There have also been few attempts to connect the time mean picture of the response to SSWs on monthly to seasonal time scales and the high-frequency (e.g., daily) North Atlantic EDJ behavior discussed above. HS14 showed that while there was a mean shift toward a more negative NAM state following a model simulated SSW, the NAM autocorrelation function was unchanged, indicating no apparent change in variability and persistence of the NAM. However, since the NAM is a hemispheric-scale quantity it does not isolate the North Atlantic EDJ behavior and its relationship to the preferred jet states.

The goal of this study is to investigate the effect of an SSW on the daily North Atlantic EDJ variability. We further relate the changes in EDJ latitude distribution to the response of the NAO. This puts the mean southward shift of the EDJ following SSWs, described extensively in the literature, into the context of changing EDJ variability and the trimodal regime framework for the North Atlantic jet. We use carefully designed climate model simulations to enable a comparison of tropospheric variability during an SSW with a state unaffected by stratospheric variability. The remainder of the paper is laid out as follows: section 2 describes the model, experiments, and diagnostics used in the study; section 3 describes the results; and section 4 summarizes our main conclusions.

2. Methods

a. Model experiments

We use experiments performed with the Canadian Middle Atmosphere Model (CMAM) described in detail by HS14. CMAM is a comprehensive global climate model (Scinocca et al. 2008) run here at T63 spectral truncation and 71 vertical levels with a model top at 0.0006 hPa (roughly 100 km). All integrations were carried out using a climatological repeated annual cycle for sea surface temperatures and sea ice (collectively, SSTs). The greenhouse gases and SSTs are held fixed at levels representative of 1990 conditions and a fixed climatological ozone field is specified in all experiments.

Two experiments will be discussed that use a "nudging" technique (see below for details): 1) a 100-yr time-slice control integration (CTRL) in which the zonal-mean state of the stratosphere is constrained to follow a seasonally evolving climatology taken from a separate 100-yr free-running CMAM simulation (this means there is little interannual zonal-mean stratospheric variability in CTRL and there are no major SSWs simulated) and 2) a 97-member ensemble of winter integrations spun off from CTRL in which the zonal mean state of the stratosphere is constrained to follow a specific reference major SSW taken from the free-running CMAM simulation. The SSW chosen as the reference case for the SSW experiment is a displacement event that occurs in late December of year 17 of the free-running simulation [see Fig. 1 of Hitchcock and Shepherd (2013), which describes the stratospheric variability in the free-running CMAM simulation]. The particular SSW event is characterized by a polar-night jet oscillation behavior (Hitchcock et al. 2013) and exhibits lower stratospheric temperature anomalies that persist for several months. The SSW experiment is referred to as "SSWd" in HS14. Each ensemble member of the SSW experiment is performed by initializing a new experiment from a reference date of 21 December in each year of the CTRL run. To reduce the effects of any initial discontinuity associated with the implementation of the nudging (see below), the first 11 days of the simulations are discarded and the analysis focuses solely on the January to March period.

As described by HS14, the nudging in the stratosphere is achieved by applying an additional relaxation on the zonal mean spectral components X of the temperature, vorticity, and divergence fields of the form $-K(p)(X - X_0)/\tau_N$, where the reference state X_0 is either the climatology X_c of the respective field from the free-running experiment or, in the SSW experiment after 21 December, the instantaneous state of the SSW from the free-running simulation X_s. Time scale τ_N is taken to be 6 h, and $K(p)$ is a height-dependent prefactor that varies between 0 and 1. The relaxation is applied only in the stratosphere, with $K(p)$ set to 0 between the surface and 68 hPa, then rising linearly to 1 at 28 hPa, and remaining at 1 at pressures of less than 28 hPa. Although the nudging is performed on model hybrid pressure levels these are very close to constant pressure surfaces in the stratosphere. The zonally asymmetric components in the stratosphere are allowed to evolve freely in both experiments. The different ensemble members of each respective experiment show a similar zonal mean

stratospheric evolution. This can be seen in Fig. 1a, which shows daily zonal mean zonal winds at 60°N and 50 hPa for a subset of 20 winters from each of the CTRL and SSW experiments. The stratospheric westerlies weaken in SSW in two phases: the first starts in late December and shows a weakening relative to CTRL of around 10 m s^{-1} at 50 hPa, and the second phase starts in mid-January and leads to weaker westerlies by around 20 m s^{-1} overall relative to CTRL. The westerlies in SSW subsequently increase starting from mid-February and reach a similar strength to CTRL by late March. The westerlies are stronger in SSW than in CTRL in April, although this period is not included in the analysis. In both the CTRL and SSW experiments the tropospheric state is unconstrained and evolves freely. This can be seen in Fig. 1b, which shows zonal mean zonal winds at 60°N and 700 hPa in the same 20 members as in Fig. 1a. There is comparatively larger variance in the troposphere among the members as a consequence of the large internal atmospheric variability at midlatitudes. There are also differences in tropospheric behavior between each member of the SSW experiment and the respective year of CTRL from which it is initialized, demonstrating that nudging to a different stratospheric state is a sufficient perturbation to lead to altered chaotic tropospheric variability in the experiments.

While the nudging constrains the zonal mean state of the stratosphere, the zonally asymmetric components are unconstrained and evolve freely. This means the nudged simulation may not lead to similar wave driving or stratospheric residual circulation as occurred during the actual SSW event simulated in the free-running experiment. The wave forcing in the free-running experiment that causes the SSW corresponds to sources and sinks of angular momentum within the stratosphere; these sources and sinks must be produced in the nudged simulation in order to constrain the zonal mean flow leading to nonconservation on angular momentum (e.g., Shepherd and Shaw 2004; Chrysanthou et al. 2019). HS14 showed there are marked differences in the stratospheric Eliassen–Palm flux divergence between the SSW generated in the free-running simulation and the SSW nudged ensemble. This is associated with differences in the meridional circulation within the nudging region (i.e., in the stratosphere), but below the level of the nudging (i.e., in the troposphere) the residual circulation induced by the nudging closely resembles that produced by the stratospheric forcing in the freely simulated stratospheric event (Hitchcock and Haynes 2014). Therefore any coupling between the stratosphere and troposphere induced 1) through the mean meridional circulation or 2) through the response of tropospheric eddies to lower-stratosphere perturbations

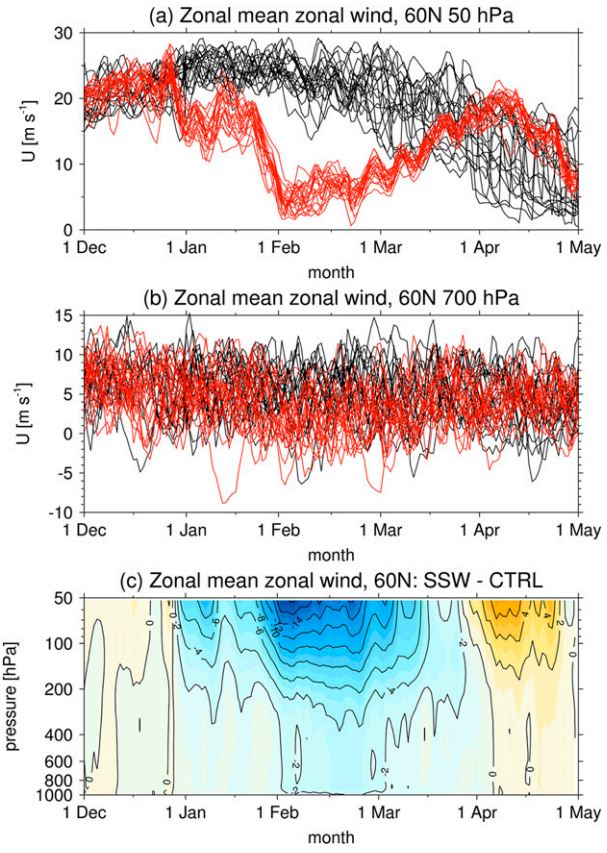

FIG. 1. A 20-member sample of daily zonal mean zonal wind (m s^{-1}) from the CTRL (black) and SSW (red) experiments at (a) 50 and (b) 700 hPa. This shows that the stratosphere follows the same broad evolution in the experiments because of nudging but the troposphere evolves freely. (c) Time–pressure cross section of the difference in ensemble mean zonal mean zonal wind at 60°N (m s^{-1}) between the SSW and CTRL experiments. Solid contours are plotted at 2 m s^{-1} intervals.

will be captured in the SSW ensemble. As explained above, the correct zonal asymmetries associated with the initial displacement of the vortex at short lags are not included as part of the nudging, and therefore coupling mechanisms that are dependent on specific features of the stratospheric zonal asymmetry around the SSW onset will not be active. However, over sufficiently large sample sizes the surface signatures of split and displacement SSWs have been shown to be comparable (Maycock and Hitchcock 2015) and various measures of the surface climate response in the SSW experiment have been shown to agree with reanalysis data (HS14).

b. Jet latitude diagnostics

Following Woollings et al. (2010a) the jet latitude index is calculated as the latitude of the maximum lower tropospheric mean (930–700 hPa) zonal wind between 20° and 75°N averaged over the North Atlantic sector

(60°W–0°). Woollings et al. (2010a) show that the longitudinally averaged jet latitude index exhibits a similar multimodal latitudinal structure to a two-dimensional North Atlantic jet index, despite the jet showing a southwest–northeast tilt. The zonal winds are first interpolated from the model grid onto a regular 0.2° latitude grid using a four-point cubic spline interpolation. The jet latitude index is then defined as the location of the maximum zonal wind speed. Woollings et al. (2010a) apply a 10-day low-pass filter to the wind profiles before calculating the jet latitude index; while they state this does not strongly affect their results, we do not apply a time filter to the winds because we also analyze persistence characteristics of the jet latitude index and this is most cleanly done using the raw wind fields. We do not find a strong annual cycle in jet latitude index over the 3-month analysis period [January–March (JFM)] and hence for clearer interpretation we show the absolute jet latitude rather than anomalies.

Following Frame et al. (2011) cluster analysis of the jet latitude index is performed using a *k*-means cluster algorithm applied to the combined CTRL and SSW datasets specifying 3 degrees of freedom. The cluster algorithm was applied separately to the two datasets, but the resulting cluster centroids and associated zonal wind profiles were found to be similar in the two experiments (i.e., the difference in centroid locations of the two cluster sets is much smaller than the Euclidian distance between clusters). Hence to avoid issues with distinguishing differences in cluster behavior from small differences in the cluster centroids between the experiments, the results presented use cluster centroids derived from the combined CTRL + SSW dataset ($n = 90 \times 197 = 17730$).

c. Comparison with reanalysis data

We compare the SSW and CTRL jet latitude distributions from CMAM with the JRA-55 reanalysis dataset (Kobayashi et al. 2015; acronym expansions can be found at https://www.ametsoc.org/PubsAcronymList). Central dates for SSWs in JRA-55 starting from 1 January 1958 are taken from Butler et al. (2017), which gives a total of 36 major warmings between November and March. We composite the jet latitude index for days 10–40 after the central date of each SSW to produce an $\mathrm{SSW}_{\mathrm{rean}}$ distribution. Note that in the reanalysis the SSWs occur at different times in the winter, whereas the ensemble members of the SSW experiment follow a similar evolution with the SSW onset at the same time. To develop a reference jet latitude distribution for the reanalysis ($\mathrm{CTRL}_{\mathrm{rean}}$) that is as comparable to CTRL as possible, we sample the equivalent dates for other years in the reanalysis that are not classified as post-SSW days 10–40.

d. Dynamical diagnostics

To interpret the behavior of the different jet latitude clusters we use several dynamical diagnostics following Novak et al. (2015), who applied these to a reanalysis dataset. The diagnostics are 1) the relative angular momentum averaged between 0° and 30°W and across 930–700 hPa, which represents latitudinally weighted lower-level zonal wind ($r = ua\cos\phi$, where ϕ is latitude); 2) the low-level meridional eddy heat flux ($\overline{v'T'}$) averaged between 40° and 70°W and across 930–700 hPa, where primes denote departures from the zonal mean and the fields are prefiltered with a Lanczos bandpass filter with a width of 30 days to remove frequencies lower than 10 days; and 3) the low-level Eady growth rate σ, used as a measure of baroclinicity, averaged between 30° and 90°W and calculated across the layer 972–700 hPa:

$$\sigma = 0.31\frac{f}{N}\frac{du}{dz}, \tag{1}$$

where f is the Coriolis parameter, N is the static stability, u is the zonal wind, and z is height. These diagnostics are chosen to allow a comparison of the CMAM experiments with results from reanalysis data described by Novak et al. (2015).

e. Calculation of leading modes

In section 3e the changes in jet latitude are compared to the leading patterns of circulation variability defined as the first two empirical orthogonal functions (EOFs) of North Atlantic sea level pressure in the region $20° \le \phi \le 90°$ and 90°W ≤ longitude $\lambda \le 40$°E. To reduce the effects of high-frequency variability on the determination of the leading patterns, the EOFs are computed using JFM monthly mean sea level pressure (SLP) anomalies from the CTRL experiment. The EOFs derived for JFM in the CTRL experiment are very similar to those calculated for DJF season and to those calculated using the SSW experiment data (not shown). The daily SLP anomalies from each experiment are then projected onto the two leading patterns to derive daily principal component time series. This approach means that amplitude of the daily principal components is larger than normal (i.e., up to ±6 std dev), but the relative changes can be compared between the experiments.

f. Calculation of uncertainties

Where appropriate, uncertainties on the results are assessed using bootstrap sampling with replacement. For the model simulations, 5000 random N-member samples are taken and the 95% confidence intervals are plotted as the 2.5th–97.5th percentiles of the sample

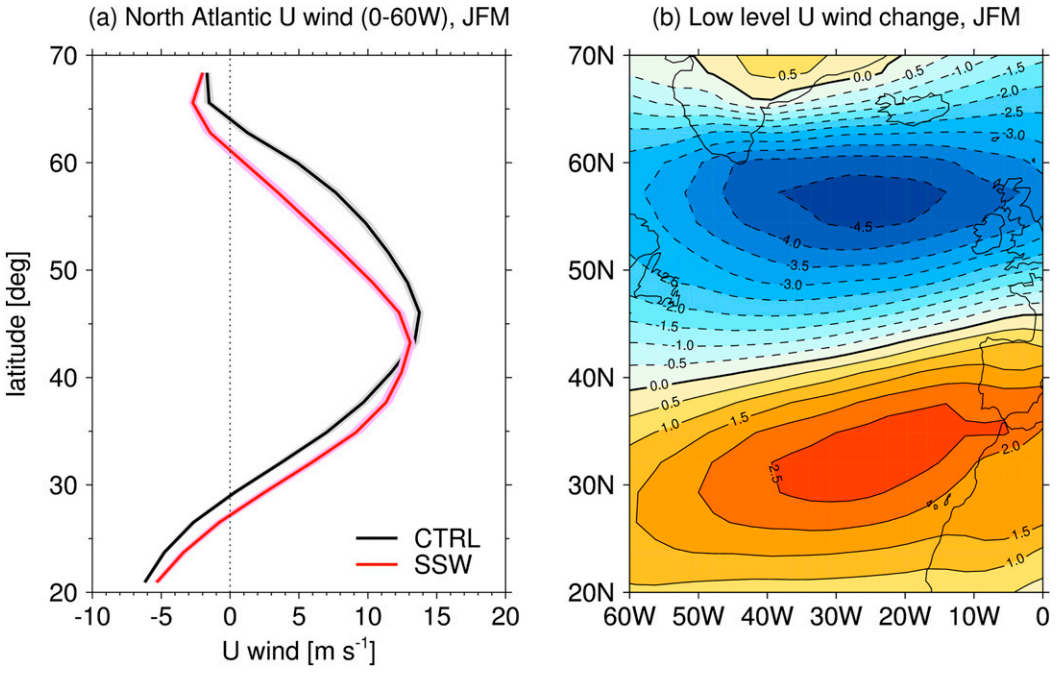

FIG. 2. (a) Latitude profile of the low-level JFM zonal wind averaged over the North Atlantic sector and between 930 and 698 hPa in the CTRL (black) and SSW (red) experiments. Shading shows 2.5th–97.5th percentiles of $n = 5000$ bootstrapping with replacement. (b) Differences in JFM zonal wind over the North Atlantic sector between the SSW and CTRL experiments. The contour interval is 0.5 m s^{-1}.

distribution, where N is the ensemble size for the CTRL or SSW experiment.

For the JRA-55 reanalysis data, since the sampled SSWs occur at different times in the winter, the bootstrap distribution is constructed by randomly sampling 1000 times N_i sets of dates corresponding to days 10–40 following each observed SSW i, but taken from winters without an SSW. $N = 36$ is the number of observed SSWs in the JRA-55 reanalysis between 1958 and 2014, as listed by Butler et al. (2017). This gives uncertainty estimates that account for the same sampling of the seasonal cycle in jet latitude index as the $\mathrm{SSW}_{\mathrm{rean}}$ distribution.

3. Results

a. Changes in zonal winds across the season

Figure 1c shows differences in daily zonal mean zonal wind at 60°N between the SSW and CTRL experiments as a function of pressure and time. As described by HS14, and as shown in Fig. 1a, the SSW begins in late December and induces stratospheric easterly anomalies that persist in the lower stratosphere until the end of March. Easterly anomalies are also simulated throughout the depth of the troposphere between January and March (also Fig. 1b). This is the canonical picture of the response to major SSWs but note this is particularly clear in this example given the relatively large ensemble size.

In the lower troposphere, the JFM average low-level zonal wind anomalies over the North Atlantic Ocean show a dipole structure in latitude (Fig. 2b), with easterly anomalies in the northern part of the basin and westerly anomalies to the south. This corresponds to a southern shift of the westerly wind belt in the North Atlantic and a southward shift of the EDJ (Fig. 2a). The node where the zonal wind anomalies change sign has a northeast tilt being around 40°N in the western North Atlantic and 47°N in the eastern side of the basin (Fig. 2b), which resembles the tilt of the EDJ itself (not shown). The peak-to-peak dipole in North Atlantic zonal winds has an amplitude of 6.4 m s^{-1}, with the decrease in zonal winds to the north around double the increase in the south. This asymmetry means the jet speed decreases by around 0.8 m s^{-1} in the SSW experiment. The relative angular momentum ($r = ua\cos\phi$) shows a more symmetric dipole in latitude (not shown), indicating that following the SSW angular momentum is predominantly being redistributed within the North Atlantic sector rather than through remote exchanges with other regions.

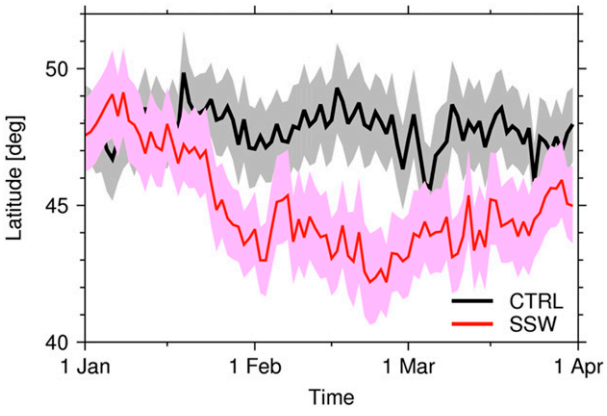

FIG. 3. Time series of daily ensemble mean North Atlantic jet latitude (°) from January to March for the SSW (red) and CTRL (black) experiments. The shading shows 2.5th–97.5th percentiles of $n = 5000$ bootstrapping with replacement.

b. *Changes in North Atlantic jet latitude index*

The evolution of the ensemble mean daily North Atlantic EDJ latitude index shows no significant differences between the SSW and CTRL experiments in early January (Fig. 3), but from mid-January onward there is a clear southward shift of the EDJ in the SSW experiment which is not seen in CTRL. Between mid-January and early February in the SSW experiment the EDJ rapidly moves equatorward, on average, by around 4° latitude. The EDJ then remains farther equatorward during February before it begins from late February onward to gradually return poleward by around 3°, but it is still located farther south than in CTRL by the end of March. The difference in ensemble mean jet latitude index ($\overline{\Delta\phi_{\mathrm{JLI}}}$) across all JFM days is −2.8° (~310 km).

The black line in Fig. 4a shows the histogram of daily JFM North Atlantic jet latitude index in the CTRL experiment for all ensemble members. The distribution is non-Gaussian and exhibits broadly similar maxima to those seen in reanalysis data (Barnes and Hartmann 2010a; Woollings et al. 2010a). There is a central (*C*) maximum around 45°N, a broader northern (*N*) maximum between 50°–63°N and a southern maximum (*S*) between 35°–40°N. The most striking difference relative to reanalysis data is that the *N* and *S* states do not occur as frequently in CMAM, which is a feature also seen in other climate models with similar atmospheric horizontal resolutions (Iqbal et al. 2018).

Also shown in Fig. 4a is the daily jet latitude index for the SSW experiment (red line). This shows a markedly different distribution from the CTRL experiment. The relative frequency of the *S* maximum increases and the *N* and *C* maxima decrease. Hence, the mean southward shift of the North Atlantic EDJ following the SSW (Figs. 2 and 3) is a manifestation of a redistribution of the daily jet latitude from fewer *N* and *C* jet states to an increase in *S* jet states. This is in contrast to what would arise with an overall southward shift of the jet latitude distribution, as can be seen by comparing the SSW jet latitude distribution with the CTRL distribution shifted by the mean SSW–CTRL jet latitude index anomaly ($\overline{\Delta\phi_{\mathrm{JLI}}} = -2.8°$) (thin black line in Fig. 4b). This shows clearly that the mean response of the EDJ following the SSW projects onto the underlying multimodal jet latitude distribution and suggests changes to the jet variability. This is distinct from the perspective of changes in the NAM in the SSW experiment, which shows a uniform shift of the distribution toward more negative values with little change in variance or persistence (see Fig. 6 of HS14).

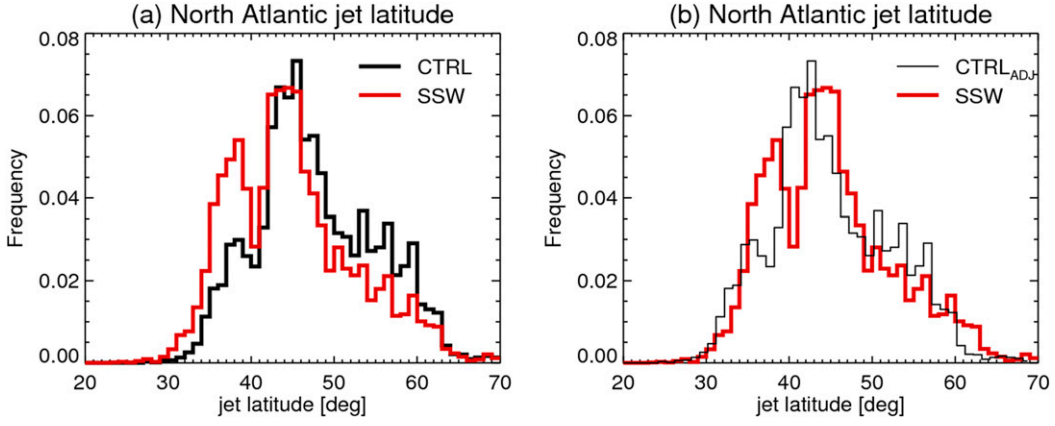

FIG. 4. Histograms of daily JFM North Atlantic jet latitude in the (a) SSW (red) and CTRL (black) experiments and (b) the SSW experiment and the CTRL distribution shifted by $\overline{\Delta\phi_{\mathrm{JLI}}}$.

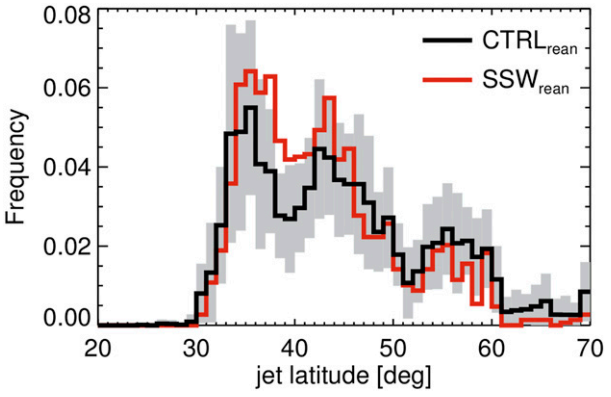

FIG. 5. Histograms of the daily North Atlantic jet latitude from the JRA-55 reanalysis dataset. The red line (SSW$_{rean}$) shows the composite of days 10–40 following the 36 major SSWs identified since 1 Jan 1958 in the reanalysis (Butler et al. 2017). The thick black line (CTRL$_{rean}$) shows the mean of the reference non-SSW bootstrap samples (n = 1000) for the same dates as the SSWs. The gray shading shows ±1 std dev of the CTRL$_{rean}$ bootstrap samples (see section 2 for details).

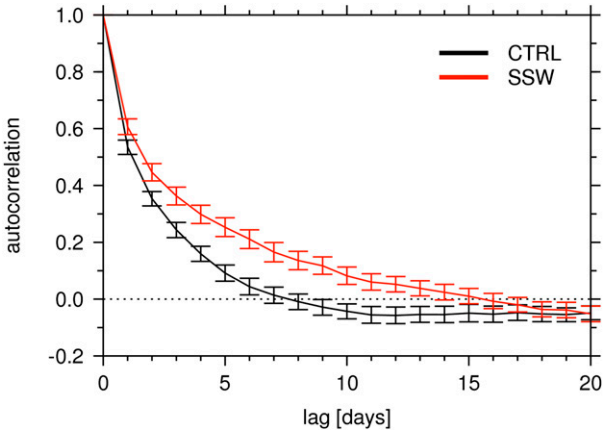

FIG. 6. The autocorrelation function of North Atlantic jet latitude in the CTRL (black) and SSW (red) experiments. Error bars show 2.5th–97.5th percentiles of n = 5000 bootstrapping with replacement.

Figure 5 shows histograms of the jet latitude index for SSW and non-SSW periods from JRA-55 based on the methods described in section 2c. The solid black line denotes the mean for each bin of the CTRL$_{rean}$ bootstrap samples, and the gray shading shows ±1 standard deviation. The red line denotes the distribution for days 10–40 after the 36 major SSWs in the dataset (SSW$_{rean}$). Given the smaller sample size, along with other differences such as the magnitude, persistence, and timing of the SSWs, the differences between SSW$_{rean}$ and CTRL$_{rean}$ are not statistically significant for most latitude bins. Nevertheless, the results suggest qualitatively similar behavior to that found in CMAM, with an increased likelihood of the jet being located at more southerly latitudes following SSWs. Indeed, around 35°–40°N there is less than a 10% chance that without SSWs the probability of the jet being at that location would be as high as in SSW$_{rean}$.

c. *Changes in EDJ persistence*

Figure 6 shows the autocorrelation function (ACF) of the jet latitude index in the two CMAM experiments. The jet latitude index shows enhanced persistence in the SSW experiment at lags of up to around two weeks. This behavior is distinct from the NAM ACF in these experiments (see Fig. 6b of HS14), which shows no significant difference between CTRL and SSW. There is also a suggestion of the ACF being somewhat flatter than in the CTRL experiment between days 5 and 10. The lag at which the ACF falls below 1/e increases from day 2 in the CTRL experiment to day 3 in the SSW experiment. This appears to be consistent with other studies that show that the S regime is more persistent than the N regime (Barnes and Hartmann 2010a; Frame et al. 2011), and hence an increase in occurrence of the S state would tend to lead to an overall increase in persistence of the jet. It is possible there may also be changes to the persistence characteristics of the regimes themselves and this is addressed next.

To examine the changes in persistence of the North Atlantic EDJ in the SSW experiment further, we apply a k-means cluster analysis to the combined (CTRL + SSW) dataset of JFM daily North Atlantic zonal wind profiles from both experiments following the method of Frame et al. (2011) and specifying three degrees of freedom (see section 2b). The North Atlantic zonal wind profiles associated with the three cluster centroids (N, C, and S) are shown in Fig. 7. The north (N) centroid shows the broadest region of westerlies between 30° and 70°N and the weakest zonal wind maximum of 11 m s^{-1}. The central (C) centroid shows a stronger zonal wind maximum of ~15 m s^{-1} located between 45° to 50°N. The south (S) centroid shows a slightly stronger zonal wind maximum of around 16 m s^{-1} near 40°N. These maxima closely align with the peaks in the jet latitude index distribution in Fig. 4, suggesting that the cluster analysis has identified the zonal wind profiles that are associated with the dominant regimes of jet latitude variability. Overall the zonal wind profiles for the three cluster centroids are comparable with those derived from reanalysis data (cf. Fig. 1 in Frame et al. 2011). The main differences are that in reanalysis data the wind maximum in the N centroid is located farther north than in CMAM near 60°N, and the C centroid shows a stronger zonal wind maximum (~15 m s^{-1}) relative to the S centroid (~12 m s^{-1}).

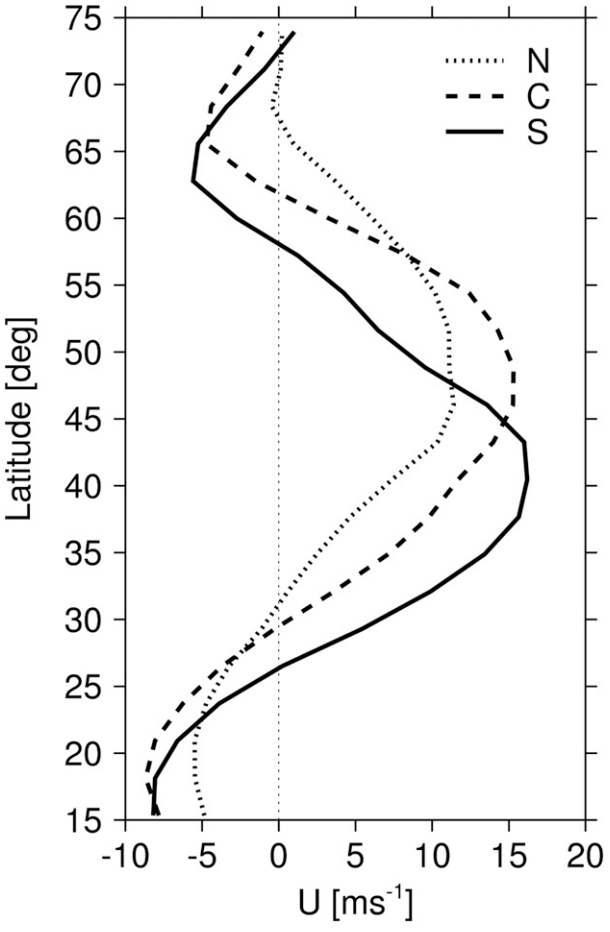

FIG. 7. North Atlantic mean zonal wind profiles (m s^{-1}) associated with the south (solid), central (dashed), and (c) north (dotted) jet clusters.

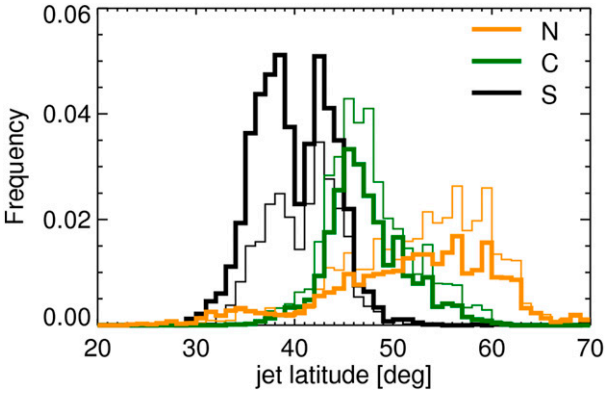

FIG. 8. Histograms of daily JFM North Atlantic jet latitude associated with the north (yellow), central (green), and south (black) clusters. Thin lines show the CTRL, and thick lines show the SSW experiment.

Following Frame et al. (2011), we assign each JFM daily wind profile for each ensemble member, $U(\phi, t)$, to one of the three clusters based on the cluster zonal wind profile $U_c(\phi)$ (Fig. 6) that is closest to it in the squared Euclidian norm:

$$|U - U_c|^2 = \sum_{\phi=\phi_1}^{\phi_2} [U(\phi, t) - U_c(\phi)]^2. \quad (2)$$

The result is an indicator variable X_t that takes on values of N, C, or S depending on to which cluster the jet belongs at time t:

$$X_t[U(\phi, t)] = \underset{c=N,C,S}{\text{argmin}}(|U - U_c|^2). \quad (3)$$

Histograms of the jet latitude index for the days assigned to each cluster are shown in Fig. 8 for the SSW and CTRL experiments. This confirms that the peaks in the jet latitude index distributions (Fig. 4a) are most frequently associated with each of the three cluster centroids (Fig. 7). The relative frequencies of the three clusters (N, C, and S) for the two experiments are shown in Table 1. The occurrence of both the N and C states each decrease by around 10% in the SSW experiment and the S state increases by ~20%, representing around ½ of all JFM days. Charlton-Perez et al. (2018) found that following weak vortex days the likelihood of a negative NAO state increased by around a factor of 2 relative to neutral vortex days, bringing it to approximately ⅓. We return to the relationship between the change in EDJ latitude distribution and the NAO in section 3e.

To examine the relationship between the changes in cluster frequency (Table 1) and the changes in jet latitude persistence (Fig. 5), we adopt the statistical approach described by Frame et al. (2011) to examine transitions between clusters. We define a lagged conditional probability of the form

$$P_{A\to B}(\tau) = P(X_{t+\tau} = B | X_t = A). \quad (4)$$

In practice this is computed by counting, at day t, all days that occupy cluster A (N_A); we then compute the fraction of those points that occupy cluster B (N_B) at a later time $t = t + \tau$, such that $P_{A\to B} = N_B/N_A$. Uncertainties are derived from a bootstrapping sampling with replacement of $P_{A\to B}$ across the different ensemble members of the experiments. The measure $P_{A\to B}$ takes

TABLE 1. Percentage occurrence of each daily jet cluster in the different experiments.

Cluster expt	S	C	N
CTRL	27	36	37
SSW	48	25	27

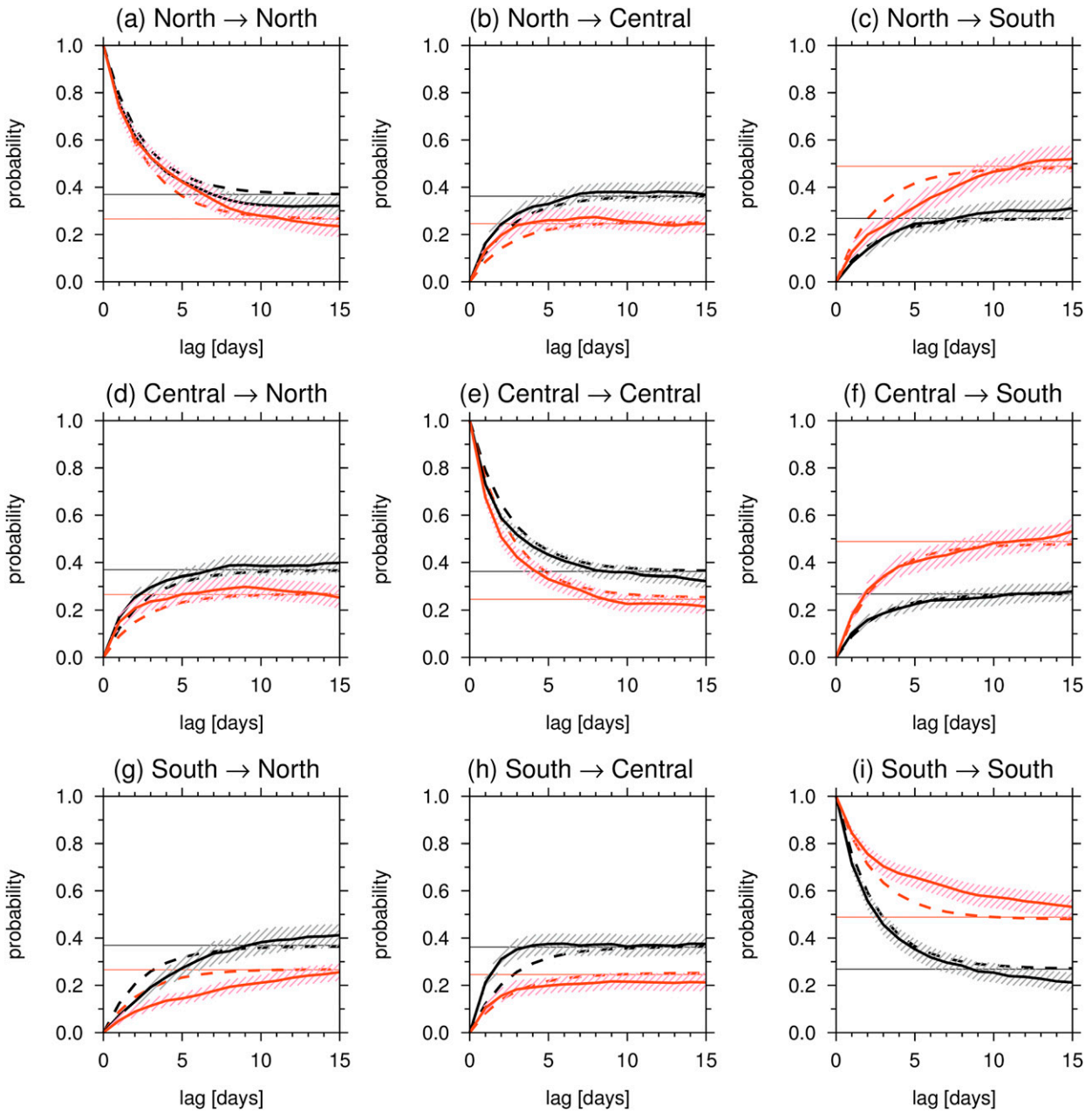

FIG. 9. Jet transition probabilities $P_{X\to Y}$ as a function of lead time for the SSW (red) and CTRL (black) experiments following Frame et al. (2011). Hatching shows 2.5th–97.5th percentiles of $n = 5000$ bootstrapping with replacement. The horizontal lines represent the climatological cluster occupancy in each experiment. Rows show transitions for states from the (top) north, (middle) central, and (bottom) south clusters. Columns show transitions to (left) north, (center) central, and (right) south clusters. For example, the top-left panel shows $P_{N\to N}$ and the lower-right panel shows $P_{S\to S}$. The dashed lines show the expected transition probabilities in the two experiments on the basis of a 1 million–step Markov chain Monte Carlo model applied to the steady-state transition matrices.

no account of the cluster occupancy between time t and $t + \tau$. However, over short time scales one can loosely interpret $P_{A\to A}$ as being the probability of a state A persisting for τ days and $P_{A\to B}$ as being the probability of a state A transitioning to state B over a time τ; we henceforth call this quantity a transition probability. Figure 9 shows the transition probabilities between the N, C, and S clusters in the two experiments for lags up to 15 days. Given there are differences in the climatological occupancy of the clusters between the two experiments (Table 1), we would expect to see differences in the transition probabilities even in the absence of any

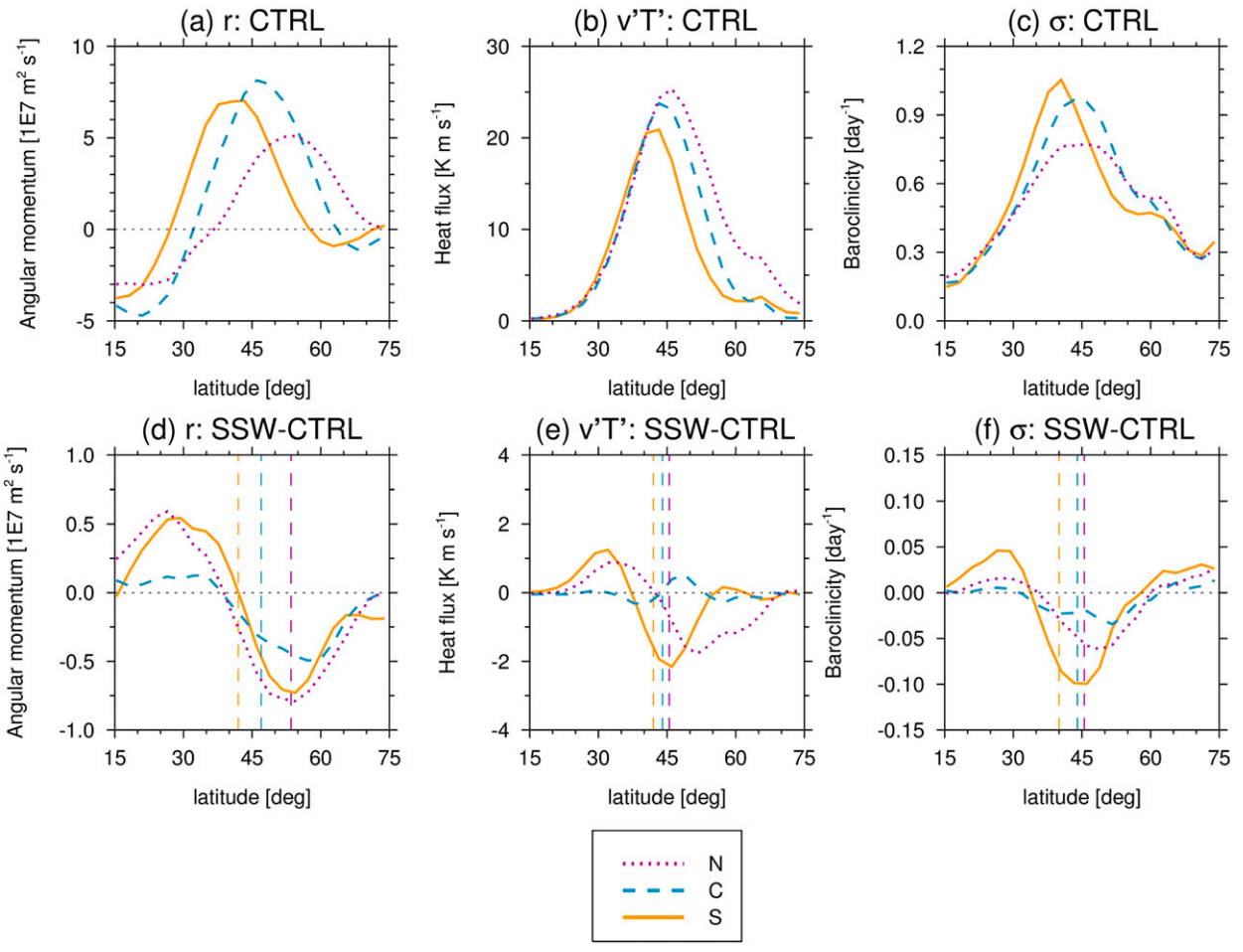

FIG. 10. Composites of latitudinal profiles of the (a),(d) low-level relative angular momentum ($m^2\,s^{-1}$; averaged between 0° and 30°W), (b),(e) the low-level eddy heat flux (K $m\,s^{-1}$; averaged between 40° and 70°W), and (c),(f) the low-level baroclinicity σ (day^{-1}; averaged between 30° and 90°W) for the (top) CTRL experiment and (bottom) SSW − CTRL differences. Values are plotted for the *N* (pink dotted), *C* (blue dashed), and *S* (yellow solid) EDJ clusters. Vertical lines in (d)–(f) show the locations of the maxima for each variable and cluster in CTRL [(a)–(c)].

meaningful changes in the dynamical system. To distinguish this effect from any potential signal from changes in dynamical behavior of the regimes, we compare the transition probabilities from the experiments with a simple one-step three state Markov model. The steady-state transition matrices for the Markov model are

$$\lim_{N\to\infty}\mathbf{P}^N = \begin{bmatrix} 0.37 & 0.36 & 0.27 \\ 0.37 & 0.36 & 0.27 \\ 0.37 & 0.36 & 0.27 \end{bmatrix}$$

for the CTRL experiment and

$$\lim_{N\to\infty}\mathbf{P}^N = \begin{bmatrix} 0.27 & 0.25 & 0.48 \\ 0.27 & 0.25 & 0.48 \\ 0.27 & 0.25 & 0.48 \end{bmatrix}$$

for the SSW experiment (Table 1). The Markov models fit to the two experiments using the steady-state transition matrices are shown by the dashed lines in Fig. 9. For a positive recurrent Markov chain, the mean recurrence time is given by the reciprocal of the steady state probability. Hence the recurrence time for the *S* regime is approximately 4 days in the CTRL experiment ($P_S = 0.27$; $1/P_S = 3.7$) and 2 days in the SSW experiment ($P_S = 0.48$; $1/P_S = 2.1$).

The results in Fig. 9 show that, in many cases, the differences in transition probabilities between the SSW and CTRL experiments are consistent with those predicted by the simple Markov model, which supports the null hypothesis of there being no discernible change in the characteristics of transitions between the regimes. However, there are some notable exceptions. For the SSW experiment, the model data show a considerable

enhancement in $P_{S\to S}$ relative to the Markov chain model on 3–12-day time scales (Fig. 9i). This is balanced by a relatively lower $P_{S\to N}$ in the SSW experiment than expected from the Markov chain model (Fig. 9g), whereas there are no differences between the model data and the Markov chain model for $P_{S\to C}$ (Fig. 9h). This suggests that in the SSW experiment the jet becomes proportionately less likely to move from the *S* to the *N* cluster and is more likely to persist in the *S* cluster. Another intriguing feature of the SSW experiment is the transition probability $P_{N\to S}$ is lower than predicted by the Markov chain model on 2–8-day time scales (Fig. 9c), while $P_{N\to C}$ is slightly elevated (Fig. 9b). This suggests that when in the *N* cluster, the jet may be less likely to transition into the *S* cluster, despite the *S* cluster becoming more frequent overall in the SSW experiment. The dynamical features of the three clusters are examined in the next section in an attempt to explain the changing transition characteristics described here.

d. *Dynamical interpretation of the changes in EDJ regimes*

To seek an explanation for the differences in transition probabilities (Fig. 9), we now explore the dynamical characteristics of the EDJ clusters using the variables described in section 2d. Figures 10a–c show the relative angular momentum, the meridional heat flux, and the baroclinicity for the three EDJ clusters in the CTRL experiment. The profiles represent composites across all JFM days assigned to the *N*, *C* and *S* clusters. The profiles for the clusters in the CTRL experiment are in good agreement with the findings of Novak et al. (2015) using reanalysis data. Specifically, the *S* cluster is associated with enhanced baroclinicity and suppressed eddy heat fluxes, and vice versa for the *N* cluster. Novak et al. (2015) interpreted the differences in dynamical characteristics between the clusters as reflecting the spatio-temporal life cycle of the North Atlantic jet, where the interplay between baroclinicity, storm-track activity (heat flux), and eddy anisotropy leads to transitions between the preferred jet states.

Figures 10d–f show differences in the dynamical variables between the SSW and CTRL experiments for each cluster. For orientation, the vertical lines in Figs. 10d–f show the location of the maximum for each variable within each cluster in the CTRL experiment. The differences in relative angular momentum between SSW and CTRL (Fig. 10d) are indicative of the small differences in zonal wind profiles found when the cluster analysis is applied separately to the two experiments (see discussion in section 2b). In all cases, these show dipole anomalies with enhanced westerlies at lower latitudes and reduced westerlies at higher latitudes, particularly for the *N* and *S* clusters, consistent with an overall more equatorward jet in the SSW experiment. However, the differences in relative angular momentum between the experiments are small compared to the differences between the clusters themselves (Fig. 10a) and hence this further motivates the use of the pooled clusters.

Figure 10e shows the differences in heat flux for each cluster between the two experiments. The changes in the *C* cluster are small and will not be discussed further. In the *N* cluster, the differences show a dipole structure with the node approximately coinciding with the maximum heat flux in CTRL (pink vertical line; Fig. 10e) indicating an equatorward shift of the peak. There is a slight asymmetry in the maximum amplitudes of the positive and negative values such that, overall, there is a small decrease in the maximum heat flux of $-0.8\,\mathrm{K\,m\,s^{-1}}$ (3%) for the *N* cluster in the SSW experiment. The *S* cluster shows markedly different behavior. While there is also a dipole structure in latitude, the node is located near 37°N while the peak in the CTRL experiment is at 42°N (yellow vertical line; Fig. 10e). The largest decreases in heat flux in the *S* cluster seen in Fig. 10e are therefore located near the peak and there is a larger decrease in the maximum heat flux of $-1.5\,\mathrm{K\,m\,s^{-1}}$ (7%) accompanied by a smaller southward shift of the profile.

The baroclinicity profiles for the three clusters in the CTRL experiment (Fig. 10c) show the highest and most equatorward maximum for the *S* cluster and the lowest and most poleward maximum for the *N* cluster. The differences in baroclinicity between the SSW and CTRL experiments for each cluster are shown in Fig. 10f. Here, again, the smallest changes are found in the *C* cluster, where there is a fairly constant decrease in baroclinicity between 30° and 60°N of around $0.01–0.02\,\mathrm{day^{-1}}$. For the *N* cluster, the differences show an asymmetric dipole in latitude with positive differences between 15° and 37°N and larger negative values between 37° and 60°N. The larger decreases occur within around 5° latitude of the peak baroclinicity in CTRL (pink vertical line; Fig. 10f), which means there is an overall decrease in the maximum baroclinicity for the *N* cluster of $-0.04\,\mathrm{day^{-1}}$ (5%) and a slight narrowing of the profile. For the *S* cluster, the profile of positive and negative differences follows the same broad shape as for the *N* cluster, but the node is around 33°N on the equatorward side of the maximum baroclinicity in the CTRL experiment near 40°N. The decrease in baroclinicity peaks near 45°N and is larger ($-0.1\,\mathrm{day^{-1}}$) than the largest relative increase between 25° and 30°N ($0.05\,\mathrm{day^{-1}}$); this means there is an overall decrease in the maximum baroclinicity for the *S* cluster in the SSW experiment of $-0.08\,\mathrm{day^{-1}}$ (8%) and a small southward shift of the profile.

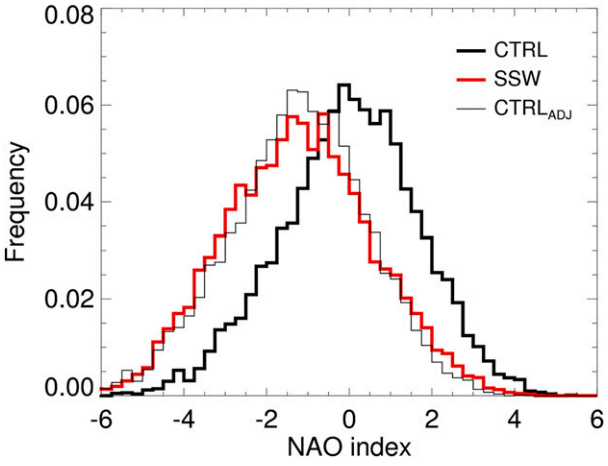

FIG. 11. Histogram of the JFM daily NAO index in the SSW (red) and CTRL (black) experiments. The thin black line shows the CTRL distribution shifted by $\overline{\Delta NAO} = -1.23$.

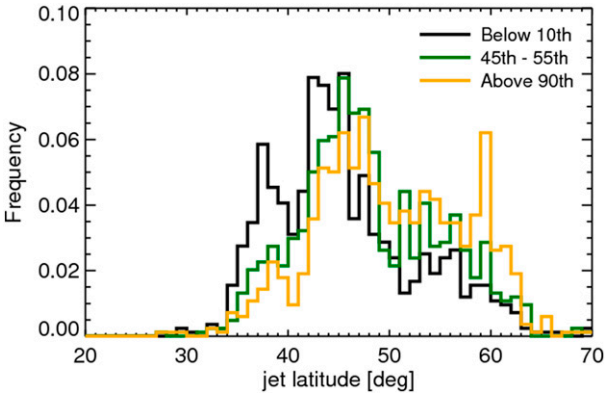

FIG. 12. Histograms of JFM daily jet latitude index corresponding to below the 10th percentile (black), between the 45th and 55th percentiles (green), and above the 90th percentile (yellow) of the NAO distribution in the CTRL experiment. The NAO percentile thresholds are determined nonparametrically.

Ambaum and Novak (2014) and Novak et al. (2015) concluded that high heat flux is conducive to a northward deflection of the EDJ, whereas low heat flux is conducive to a more zonal EDJ. The heat flux is associated with mixing of temperature gradients by eddies and gradual erosion of baroclinicity, with associated changes in eddy anisotropy and wave breaking leading to transitions between the jet regimes downstream. A possible explanation for the increased persistence of the *S* state in the SSW experiment (Fig. 9i) is that the weaker baroclinicity in the *S* cluster should lead to slower growth rates for the unstable modes. This would reduce the occurrences of explosive eddy growth, which tends to shift the jet poleward. A possible explanation for the relative delay in transition between the north and south regimes in the SSW experiment (Fig. 9c) is that the reduced baroclinicity in the north regime (Fig. 10f) makes for a slower recovery to the high baroclinicity environment that permits rapid growth of eddies associated with a southward deflected jet (Novak et al. 2015).

e. Relationship to the leading patterns

The surface response to SSWs is well known to project onto a negative NAO pattern (e.g., Charlton and Polvani 2007). This section addresses how the changes in the EDJ in the SSW experiment discussed above relate to the NAO.

Histograms of the JFM daily NAO index for the SSW and CTRL experiments are shown in Fig. 11. In the SSW experiment, the mean change in the NAO index is −1.26. Overall the CTRL distribution shifted by the change in population mean (CTRL$_{ADJ}$) compares well to the NAO distribution in the SSW experiment (thin black line; Fig. 10). The main difference is that the NAO distribution in CTRL is negatively skewed ($S = -0.18$), similar to what is found in reanalysis data (Woollings et al. 2008), but this is not the case in the SSW experiment ($S = 0.03$). A two-sample Kolmogorov–Smirnov test shows the daily NAO distributions for SSW and CTRL$_{ADJ}$ are significantly different at the 99.9% confidence level ($D = 0.034$). Woollings et al. (2008) explain the negative skewness of the daily NAO index using a two-component mixture model representing Atlantic regimes for Greenland blocking (mainly negative NAO) and a more frequent zonal state with a strong subpolar jet (mainly positive NAO). The fact that in the SSW experiment both the negative NAO skewness is reduced and the occupancy of the *S* cluster is increased is surprising, as Greenland blocking has been connected to both the existence of the *S* jet regime (Woollings et al. 2010a) and the negative skewness of the NAO (Woollings et al. 2008). One might therefore expect to find that an increase in *S* jet states would be accompanied by an increase in negative skewness of the NAO.

To further examine the relationship between jet latitude index and the NAO, Fig. 12 shows histograms of the daily jet latitude index for below the 10th percentile (NAO ≤ -2.21), between the 45th and 55th percentiles ($-0.14 \leq$ NAO ≤ 0.25) and above the 90th percentile (NAO ≥ 2.11) of the NAO distribution in the CTRL experiment. The choice of bins that encompass 10% of the CTRL distribution gives 900 days in each bin, which after some testing was found to be sufficient to sample the underlying jet latitude distribution. The percentile thresholds are determined nonparametrically using ranked probabilities of all JFM days from the CTRL

TABLE 2. Percentage daily occurrence of each jet cluster in different percentiles of the NAO distribution in the CTRL experiment.

Cluster NAO percentile	*S*	*C*	*N*
Below 10th	46	28	26
45th–55th	22	37	41
Above 90th	15	42	43

experiment. The fraction of days in each percentile category that are assigned to the three jet clusters is shown in Table 2. Around one-half of strongly negative NAO days in the CTRL experiment are assigned to the *S* cluster, with the remainder being approximately equally distributed between the *C* and *N* cluster. This confirms that the overall increase in *S* cluster frequency in the SSW experiment is consistent with the more negative NAO index. For strongly positive NAO days in the CTRL experiment, the majority of days occupy the *C* and *N* clusters approximately equally, but only around 15% of the days are classified to the *S* cluster. Figure 13 shows composite North Atlantic zonal wind profiles for the strongly negative NAO days assigned to the *N* cluster and the strongly positive NAO days assigned to the *S* cluster. These closely resemble the overall zonal wind profiles for the cluster centroids (Fig. 7). Hence while there is an overall propensity for *S* cluster jets to be associated with negative NAO days, this is not a definitive relationship (see also Fig. 11 of Woollings et al. 2010a).

Previous research has shown that more than one leading pattern is required to describe latitudinal shifts in the EDJ in both idealized models (Fyfe and Lorenz 2005; Sparrow et al. 2009) and reanalysis data (Woollings et al. 2010a). Woollings et al. (2010a) show that the North Atlantic jet latitude index captures variations in both the NAO and EA patterns. Figure 14 shows joint histograms of the daily NAO and EA indices for the SSW and CTRL experiments (cf. Fig. 11 of Woollings et al. 2010a). Figure 14 shows a shift of the joint histogram to more negative NAO values, as discussed above, but only a small change in the EA pattern ($\Delta EA_{SSW-CTRL} = 0.07$). Indeed, the change in JFM mean SLP in the SSW experiment in the North Atlantic sector can be almost entirely explained by the projection onto the NAO pattern (not shown). This is consistent with previous studies that show the SLP response to SSWs in the North Atlantic sector resembles a negative NAO (e.g., Charlton and Polvani 2007; HS14) and that stratospheric variability does not strongly affect North Atlantic weather regimes that are independent of the NAO (Beerli and Grams 2019).

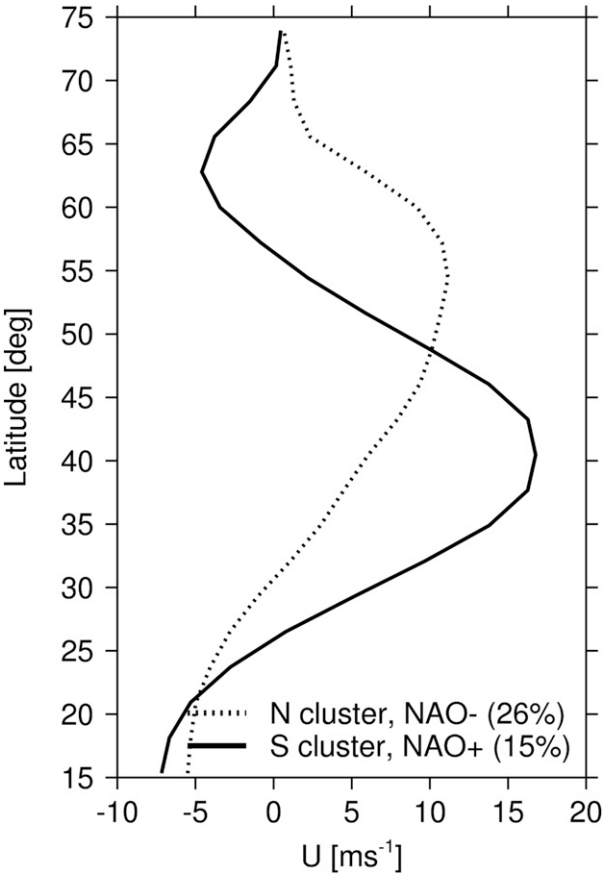

FIG. 13. Composite North Atlantic zonal wind profiles ($m\,s^{-1}$) for the subset (15%) of days with NAO above the 90th percentile and that are classified to the *S* regime (solid). Also plotted is the subset (26%) of days with NAO below the 10th percentile and that are classified to the *N* regime (dotted). The data are taken from the CTRL experiment.

4. Conclusions

This study has investigated changes in North Atlantic eddy-driven jet regimes following a major sudden stratospheric warming. We use experiments with the Canadian Middle Atmosphere Model described by Hitchcock and Simpson (2014) in which the zonal mean stratospheric state is nudged to a seasonally evolving long-term climatology (i.e., weak stratospheric variability, denoted CTRL) and to a single displacement type major SSW simulated by CMAM (denoted SSW). Both experiments are composed of a large ensemble (100 and 97 winters, respectively) and the troposphere evolves freely, thereby offering a unique opportunity to examine tropospheric variability in the presence of similar stratospheric conditions. This approach is attractive since in reanalysis data there are relatively fewer SSWs and their timing, amplitude, and persistence characteristics vary considerably, which may affect

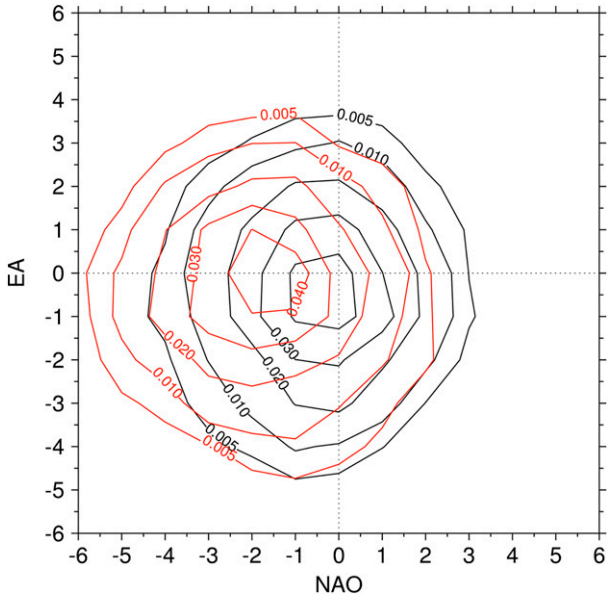

FIG. 14. Joint histogram of daily JFM NAO–EA indices in the CTRL (black) and SSW (red) experiments. The difference in the population mean NAO index is −1.23, and the difference in the EA index is 0.07. Contours are plotted at densities of 0.005, 0.01, 0.02, 0.03, and 0.04. The densities sum to 1.

the subsequent evolution in the troposphere (e.g., Karpechko et al. 2017). However, this does mean the results described here may be somewhat specific to the event simulated in CMAM. Nevertheless, HS14 analyzed an ensemble experiment for a different split type SSW event from CMAM and found very similar behavior to the SSW analyzed here. We also analyze a reanalysis dataset and find qualitatively similar behavior to the model.

CMAM produces a trimodal winter North Atlantic jet latitude distribution, although in the CTRL experiment the occurrence of the southward (*S*) and northward (*N*) regimes is relatively lower and the occurrence of the central (*C*) regime is relatively higher when compared with reanalysis data. The biases in the jet latitude distribution in CMAM are not as severe as found in some models with similar atmospheric resolutions (Iqbal et al. 2018). Following the onset of the modeled SSW in late December, the North Atlantic jet shifts south by an average of −2.8° latitude between January and March. This is associated with a redistribution of the daily jet latitude distribution within the three regimes, with an increased occurrence of the *S* regime by ~75% relative to the CTRL experiment. Alongside, there are roughly equal decreases in the frequency of the *C* and *N* jet regimes. Qualitatively similar behavior is found for a composite of 36 major sudden warmings in the JRA-55 reanalysis dataset. The higher occurrence of the *S* state in the SSW experiment is further accompanied by an increase in the persistence of the *S* regime compared to the prediction of a simple one-step Markov chain model. Under typical conditions the high heat flux associated with the *S* regime is associated with an erosion of baroclinicity that drives changes in eddy anisotropy and shifts in jet latitude (Novak et al. 2015). We suggest the increased persistence of the *S* regime may be a consequence of the decreased baroclinicity in the SSW experiment, which causes slower growth of the unstable modes, weaker eddy heat fluxes, and a lower tendency for anticyclonic wave breaking.

The sea level pressure response in the North Atlantic in the SSW experiment projects strongly onto a negative NAO pattern ($\overline{\Delta \mathrm{NAO}} = -1.23$), with little change in the EA pattern. This is interesting because intrinsic variations in jet latitude in the CTRL experiment, similar to the differences found in the SSW experiment, describe fluctuations in both the NAO and East Atlantic patterns (see also Woollings et al. 2010a). Charlton-Perez et al. (2018) used reanalysis data and ECMWF ensemble forecasts to analyze the stratospheric influence on the occurrence of winter North Atlantic weather regimes. Our results are in agreement with their main conclusions that the North Atlantic response to a weak polar vortex projects onto NAO− and that changes in the North Atlantic circulation come about through changes to both regime persistence and transitions between regimes. Further research is required to better connect the jet latitude regimes with the weather regimes in the North Atlantic.

This study makes a first attempt to connect the time mean surface response to SSWs with the regime behavior of the North Atlantic eddy-driven jet and provides a complementary approach to other work that focuses on storm-track and jet variability. For example, previous studies have related jet regimes to the leading modes of variability, such as the NAO (e.g., Woollings et al. 2008, 2011), and two studies have related the surface response to stratospheric anomalies to daily weather regimes (Charlton-Perez et al. 2018; Beerli et al. 2017). We have attempted to bridge the traditional view of a time-averaged NAO− response and southward shift of the jet following SSWs with the characteristics of daily EDJ variability. Further work could connect this with the dynamical mechanisms for stratosphere–troposphere coupling described in the literature [see Kidston et al. (2015) and references therein].

Acknowledgments. Author Maycock acknowledges funding from the Natural Environment Research Council (Grant NE/M018199/1) and the Leverhulme Trust. Some of this work was conducted while author

Masukwedza was undertaking an MRes Climate and Atmospheric Science degree in the School of Earth and Environment at the University of Leeds. We thank Andrew Charlton-Perez and two anonymous reviewers for their constructive comments, which improved the paper. The National Center for Atmospheric Research is sponsored by the National Science Foundation.

REFERENCES

Ambaum, M. H. P., 2008: Unimodality of wave amplitude in the Northern Hemisphere. *J. Atmos. Sci.*, **65**, 1077–1086, https://doi.org/10.1175/2007JAS2298.1.

——, and L. Novak, 2014: A nonlinear oscillator describing storm track variability. *Quart. J. Roy. Meteor. Soc.*, **140**, 2680–2684, https://doi.org/10.1002/qj.2352.

——, B. J. Hoskins, and D. B. Stephenson, 2001: Arctic oscillation or North Atlantic Oscillation? *J. Climate*, **14**, 3495–3507, https://doi.org/10.1175/1520-0442(2001)014<3495:AOONAO>2.0.CO;2.

Baldwin, M. P., and T. J. Dunkerton, 2001: Stratospheric harbingers of anomalous weather regimes. *Science*, **294**, 581–584, https://doi.org/10.1126/science.1063315.

Barnes, E. A., and D. L. Hartmann, 2010a: Influence of eddy-driven jet latitude on North Atlantic jet persistence and blocking frequency in CMIP3 integrations. *Geophys. Res. Lett.*, **37**, L23802, https://doi.org/10.1029/2010GL045700.

——, and ——, 2010b: Dynamical feedbacks and the persistence of the NAO. *J. Atmos. Sci.*, **67**, 851–865, https://doi.org/10.1175/2009JAS3193.1.

——, ——, D. M. W. Frierson, and J. Kidston, 2010: Effect of latitude on the persistence of eddy-driven jets. *Geophys. Res. Lett.*, **37**, L11804, https://doi.org/10.1029/2010GL043199.

Beerli, R., and C. M. Grams, 2019: Stratospheric modulation of the large-scale circulation in the Atlantic–European region and its implications for surface weather events. *Quart. J. Roy. Meteor. Soc.*, **145**, 3732–3750, https://doi.org/10.1002/qj.3653.

——, H. Wernli, and C. M. Grams, 2017: Does the lower stratosphere provide predictability for month-ahead wind electricity generation in Europe? *Quart. J. Roy. Meteor. Soc.*, **143**, 3025–3036, https://doi.org/10.1002/qj.3158.

Butler, A. H., J. P. Sjoberg, D. J. Seidel, and K. H. Rosenlof, 2017: A sudden stratospheric warming compendium. *Earth Syst. Sci. Data*, **9**, 63–76, https://doi.org/10.5194/essd-9-63-2017.

Charlton, A. J., and L. M. Polvani, 2007: A new look at stratospheric sudden warmings. Part I: Climatology and modeling benchmarks. *J. Climate*, **20**, 449–469, https://doi.org/10.1175/JCLI3996.1.

Charlton-Perez, A. J., L. Ferranti, and R. W. Lee, 2018: The influence of the stratospheric state on North Atlantic weather regimes. *Quart. J. Roy. Meteor. Soc.*, **144**, 1140–1151, https://doi.org/10.1002/qj.3280.

Charney, J. G., and J. G. DeVore, 1979: Multiple flow equilibria in the atmosphere and blocking. *J. Atmos. Sci.*, **36**, 1205–1216, https://doi.org/10.1175/1520-0469(1979)036<1205:MFEITA>2.0.CO;2.

Chrysanthou, A., and Coauthors, 2019: The effect of atmospheric nudging on the stratospheric residual circulation in chemistry–climate models. *Atmos. Chem. Phys.*, **19**, 11 559–11 586, https://doi.org/10.5194/acp-19-11559-2019.

Corti, S., F. Molteni, and T. N. Palmer, 1999: Signature of recent climate change in frequencies of natural atmospheric circulation regimes. *Nature*, **398**, 799–802, https://doi.org/10.1038/19745.

Fereday, D. R., A. Maidens, A. Arribas, A. A. Scaife, and J. R. Knight, 2012: Seasonal forecasts of Northern Hemisphere winter 2009/10. *Environ. Res. Lett.*, **7**, 034031, https://doi.org/10.1088/1748-9326/7/3/034031.

Frame, T. H. A., M. H. P. Ambaum, S. L. J. Gray, and J. Methven, 2011: Ensemble prediction of transitions of the North Atlantic eddy-driven jet. *Quart. J. Roy. Meteor. Soc.*, **137**, 1288–1297, https://doi.org/10.1002/qj.829.

——, J. Methven, S. L. Gray, and M. H. P. Ambaum, 2013: Flow-dependent predictability of the North Atlantic jet. *Geophys. Res. Lett.*, **40**, 2411–2416, https://doi.org/10.1002/grl.50454.

Franzke, C., I. Horenko, A. J. Majda, and R. Klein, 2009: Systematic metastable atmospheric regime identification in an AGCM. *J. Atmos. Sci.*, **66**, 1997–2012, https://doi.org/10.1175/2009JAS2939.1.

——, T. Woollings, and O. Martius, 2011: Persistent circulation regimes and preferred regime transitions in the North Atlantic. *J. Atmos. Sci.*, **68**, 2809–2825, https://doi.org/10.1175/JAS-D-11-046.1.

Fyfe, J. C., and D. J. Lorenz, 2005: Characterizing midlatitude jet variability: Lessons from a simple GCM. *J. Climate*, **18**, 3400–3404, https://doi.org/10.1175/JCLI3486.1.

Gerber, E. P., C. Orbe, and L. M. Polvani, 2009: Stratospheric influence on the tropospheric circulation revealed by idealized ensemble forecasts. *Geophys. Res. Lett.*, **36**, L24801, https://doi.org/10.1029/2009GL040913.

Hannachi, A., 2007: Tropospheric planetary wave dynamics and mixture modeling: Two preferred regimes and a regime shift. *J. Atmos. Sci.*, **64**, 3521–3541, https://doi.org/10.1175/JAS4045.1.

Hitchcock, P., and T. G. Shepherd, 2013: Zonal-mean dynamics of extended recoveries from stratospheric sudden warmings. *J. Atmos. Sci.*, **70**, 688–707, https://doi.org/10.1175/JAS-D-12-0111.1.

——, and P. H. Haynes, 2014: Zonally symmetric adjustment in the presence of artificial relaxation. *J. Atmos. Sci.*, **71**, 4349–4368, https://doi.org/10.1175/JAS-D-14-0013.1.

——, and I. R. Simpson, 2014: The downward influence of stratospheric sudden warmings. *J. Atmos. Sci.*, **71**, 3856–3876, https://doi.org/10.1175/JAS-D-14-0012.1.

——, T. G. Shepherd, and G. L. Manney, 2013: Statistical characterization of Arctic polar-night jet oscillation events. *J. Climate*, **26**, 2096–2116, https://doi.org/10.1175/JCLI-D-12-00202.1.

Iqbal, W., W. N. Leung, and A. Hannachi, 2018: Analysis of the variability of the North Atlantic eddy-driven jet stream in CMIP5. *Climate Dyn.*, **51**, 235–247, https://doi.org/10.1007/s00382-017-3917-1.

Karpechko, A. Y., P. Hitchcock, D. H. Peters, and A. Schneidereit, 2017: Predictability of downward propagation of major sudden stratospheric warmings. *Quart. J. Roy. Meteor. Soc.*, **143**, 1459–1470, https://doi.org/10.1002/qj.3017.

Kidston J., A. A. Scaife, S. C. Hardiman, D. M. Mitchell, N. Butchart, M. P. Baldwin, L. J. Gray, 2015: Stratospheric influence on tropospheric jet streams, storm tracks and surface weather. *Nat. Geosci.*, **8**, 433–440, https://doi.org/10.1038/ngeo2424.

Kobayashi, S., and Coauthors, 2015: The JRA-55 Reanalysis: General specifications and basic characteristics. *J. Meteor. Soc. Japan*, **93**, 5–48, https://doi.org/10.2151/jmsj.2015-001.

Kolstad, E. W., T. Breiteig, and A. A. Scaife, 2010: The association between stratospheric weak polar vortex events and cold air outbreaks in the Northern Hemisphere. *Quart. J. Roy. Meteor. Soc.*, **136**, 886–893, https://doi.org/10.1002/qj.620.

Kushner, P. J., and L. M. Polvani, 2004: Stratosphere–troposphere coupling in a relatively simple AGCM: The role of eddies. *J. Climate*, **17**, 629–639, https://doi.org/10.1175/1520-0442(2004)017<0629:SCIARS>2.0.CO;2.

Maycock, A. C., and P. Hitchcock, 2015: Do split and displacement sudden stratospheric warmings have different annular mode signatures? *Geophys. Res. Lett.*, **42**, 10 943–10 951, https://doi.org/10.1002/2015GL066754.

Monahan, A. H., and J. C. Fyfe, 2006: On the nature of zonal jet EOFs. *J. Climate*, **19**, 6409–6424, https://doi.org/10.1175/JCLI3960.1.

Novak, L., M. H. Ambaum, and R. Tailleux, 2015: The life cycle of the North Atlantic storm track. *J. Atmos. Sci.*, **72**, 821–833, https://doi.org/10.1175/JAS-D-14-0082.1.

Orlanski, I., 2003: Bifurcation in eddy life cycles: Implications for storm track variability. *J. Atmos. Sci.*, **60**, 993–1023, https://doi.org/10.1175/1520-0469(2003)60<993:BIELCI>2.0.CO;2.

Polvani, L. M., and P. J. Kushner, 2002: Tropospheric response to stratospheric perturbations in a relatively simple general circulation model. *Geophys. Res. Lett.*, **29**, 1114, https://doi.org/10.1029/2001GL014284.

——, L. Sun, A. H. Butler, J. H. Richter, and C. Deser, 2017: Distinguishing stratospheric sudden warmings from ENSO as key drivers of wintertime climate variability over the North Atlantic and Eurasia. *J. Climate*, **30**, 1959–1969, https://doi.org/10.1175/JCLI-D-16-0277.1.

Scaife, A. A., and J. R. Knight, 2008: Ensemble simulations of the cold European winter of 2005–2006. *Quart. J. Roy. Meteor. Soc.*, **134**, 1647–1659, https://doi.org/10.1002/qj.312.

——, and Coauthors, 2016: Seasonal winter forecasts and the stratosphere. *Atmos. Sci. Lett.*, **17**, 51–56, https://doi.org/10.1002/asl.598.

Scinocca, J. F., N. A. McFarlane, M. Lazare, J. Li, and D. Plummer, 2008: Technical Note: The CCCma third generation AGCM and its extension into the middle atmosphere. *Atmos. Chem. Phys.*, **8**, 7055–7074, https://doi.org/10.5194/acp-8-7055-2008.

Shepherd, T. G., and T. A. Shaw, 2004: The angular momentum constraint on climate sensitivity and downward influence in the middle atmosphere. *J. Atmos. Sci.*, **61**, 2899–2908, https://doi.org/10.1175/JAS-3295.1.

Sigmond, M., J. F. Scinocca, V. V. Kharin, and T. G. Shepherd, 2013: Enhanced seasonal forecast skill following stratospheric sudden warmings. *Nat. Geosci.*, **6**, 98–102, https://doi.org/10.1038/ngeo1698.

Silverman, B. W., 1981: Using kernel density estimates to investigate multimodality. *J. Roy. Stat. Soc.*, **43B**, 97–99, https://doi.org/10.1111/J.2517-6161.1981.TB01155.X.

Smyth, P., K. Ide, and M. Ghil, 1999: Multiple regimes in Northern Hemisphere height fields via mixture model clustering. *J. Atmos. Sci.*, **56**, 3704–3723, https://doi.org/10.1175/1520-0469(1999)056<3704:MRINHH>2.0.CO;2.

Sparrow, S., M. Blackburn, and J. D. Haigh, 2009: Annular variability and eddy–zonal flow interactions in a simplified atmospheric GCM. Part I: Characterization of high- and low-frequency behavior. *J. Atmos. Sci.*, **66**, 3075–3094, https://doi.org/10.1175/2009JAS2953.1.

Tripathi, O. P., and Coauthors, 2015: The predictability of the extratropical stratosphere on monthly time-scales and its impact on the skill of tropospheric forecasts. *Quart. J. Roy. Meteor. Soc.*, **141**, 987–1003, https://doi.org/10.1002/qj.2432.

White, R., C. Hilgenbrink, and A. Sheshadri, 2019: The importance of Greenland in setting the northern preferred position of the North Atlantic eddy-driven jet. *Geophys. Res. Lett.*, **46**, 14 126–14 134, https://doi.org/10.1029/2019GL084780.

Woollings, T., B. Hoskins, M. Blackburn, and P. Berrisford, 2008: A new Rossby wave–breaking interpretation of the North Atlantic Oscillation. *J. Atmos. Sci.*, **65**, 609–626, https://doi.org/10.1175/2007JAS2347.1.

——, A. Hannachi, and B. Hoskins, 2010a: Variability of the North Atlantic eddy-driven jet stream. *Quart. J. Roy. Meteor. Soc.*, **136**, 856–868, https://doi.org/10.1002/qj.625.

——, ——, ——, and A. Turner, 2010b: A regime view of the North Atlantic Oscillation and its response to anthropogenic forcing. *J. Climate*, **23**, 1291–1307, https://doi.org/10.1175/2009JCLI3087.1.

——, J. G. Pinto, and J. A. Santos, 2011: Dynamical evolution of North Atlantic ridges and poleward jet stream displacements. *J. Atmos. Sci.*, **68**, 954–963, https://doi.org/10.1175/2011JAS3661.1.